Earth and Planetary Science Letters 276 (2008) 140–151

Contents lists available at ScienceDirect

Earth and Planetary Science Letters

journal homepage: www.elsevier.com/locate/epsl

Serpentinization pulse in the actively deforming Central Indian Basin

Matthias Delescluse [a,c,*], Nicolas Chamot-Rooke [a,b]

[a] Ecole normale supérieure, Laboratoire de Géologie, 24 rue Lhomond, 75005, Paris, France
[b] CNRS, UMR 8538, France
[c] Université Paris XI, Orsay, France

ARTICLE INFO

Article history:
Received 27 November 2007
Received in revised form 8 September 2008
Accepted 14 September 2008

Editor: C.P. Jaupart

PACS:
91.45.G
91.50.Ln
91.55.Jk
91.55.Ln
91.60.Hg
93.30.Nk

Keywords:
heat flow
oceanic lithosphere
deformation
active faults
friction
serpentinization
multichannel seismic

ABSTRACT

Heat flow in the actively deforming Central Indian Basin is on average 30 mW/m^2 higher than the theoretical 55 mW/m^2 heat flow expected from plate cooling of a Cretaceous oceanic lithosphere. Strong spatial correlation between the anomaly and the active thrust fault network at local (faults) and regional scales suggests two potential tectonically driven mechanisms activated at the time of initiation of deformation: friction-to-heat conversion or exothermic serpentinization. We quantitatively examine both processes using an updated geometry of the thrust fault network and simple thermal models. Friction generated heat is limited in all cases: at shallow levels, shear stresses remain small, while heat generated at deeper levels does not contribute significantly to the surface heat flow since permanent regime is not reached. In the exothermic serpentinization model, a maximum anomaly of 20 to 30 mW/m^2 is reached 2 to 6 Myr after the onset of widespread serpentinization, depending on the efficiency of the water circulation. The amount and timing of heat release can fully explain the present-day surface heat flow of the Central Indian Basin, provided vigorous hydrothermal circulation closely followed the onset of deformation. Based on a reprocessed multichannel seismic line, we suggest that faults cutting through the entire crust and across the Moho discontinuity drive water at mantle levels and trigger the exothermic serpentinization reaction. We interpret sub-Moho reflectors imaged at depths of 8 to 15 km below the top of the crust – and coinciding with the location of the maximum reaction rate coefficient of serpentinization – as serpentinization fronts. We discuss the significance of this pulse of serpentinization in terms of timing of deformation, weakening and transient rheology of the oceanic lithosphere.

1. Introduction

Anomalously high heat-flow measurements have been acquired in the northeastern Indian Ocean for decades (Pollack et al., 1993) and were promptly related to the abnormal level of intraplate seismicity recorded between the India and Australia tectonic plates (Weissel et al., 1980; Wiens et al., 1986; Stein et al., 1988). The heat-flow anomaly was shown to coincide with an area of widespread intraplate deformation that started in the late Miocene (Cochran et al., 1989). Seismic profiles (Bull and Scrutton, 1992; Chamot-Rooke et al., 1993; VanOrman et al., 1995) further imaged the highly faulted sediments, crust and mantle of the Central Indian Ocean, confirming the spatial correlation between high heat-flow and active deformation. The thermal anomaly was thus seen as a consequence of friction-to-heat conversion along deeply rooted reverse faults (Weissel et al., 1980; Geller et al., 1983; Stein et al., 1988; Gordon et al., 1990). An alternative view was immediately raised: deformation may have concentrated in areas of high thermal state and weaker rheology, the high heat flow being a cause rather than a consequence of the localization of deformation. Stein and Weissel (1990) ruled out large-scale reheating at the base of the lithosphere showing that there was no associated bathymetric swell. They further inferred that the source of additional heat had necessarily to be shallow (Geller et al., 1983; Stein et al., 1988) in order to satisfy simultaneously the present-day depth to basement, the deep seismicity (Okal, 1983) (suggesting low temperatures at depth of 30–40 km) and the high surface heat flow. The topic remained closed and rather unsolved until Verzhbitsky and Lobkovsky (1993) proposed that the required shallow heat source may relate to the exothermic serpentinization of mantle peridotites, as first mentioned in Fyfe (1974). They provided a crude estimate of the produced heat and concluded that serpentinization may be as efficient as other mechanisms to increase significantly the surface heat flow in this part of the Indian Ocean.

Substantially more data are available today: (1) Using deep seismic refraction, Louden (1995) detected a low velocity zone that he attributed to partially serpentinized clasts of peridotites in the gabbros layer at the base of the oceanic crust; (2) At the scale of the thrusts network, one

* Corresponding author. Ecole normale supérieure, Laboratoire de Géologie, 24 rue Lhomond, 75005, Paris, France.
E-mail address: delesclu@geologie.ens.fr (M. Delescluse).

0012-821X/$ – see front matter © 2008 Elsevier B.V. All rights reserved.
doi:10.1016/j.epsl.2008.09.017

detailed heat-flow profile across two major active faults was obtained during a pre-site survey of the ODP Leg 116 drilling in an area close to the Afanasy–Nikitin Seamount Chain (Cochran et al., 1989). Distribution of the observed heat flow along this profile was modeled by Ormond et al. (1995) as vigorous fluid circulation through the Bengal fan sediments, redistributing an already anomalous basal heat flow. No heat source origin is proposed to explain the ~30 mW/m^2 anomaly, but these data do confirm the link with the faults; (3) Numerous seismic reflectors have been imaged in the mantle, including deep penetrating faults. Acquired in 1991, Phèdre multichannel seismic profiles (Chamot-Rooke et al., 1993) imaged the deep geometry of the thrust faults along a 2100 km-long profile across the area. Below the ODP Leg 116 site, two fault reflectors cut across discontinuous Moho phases and reach deep into the mantle, suggesting that fluid paths do exist at sub-Moho depth. Deep

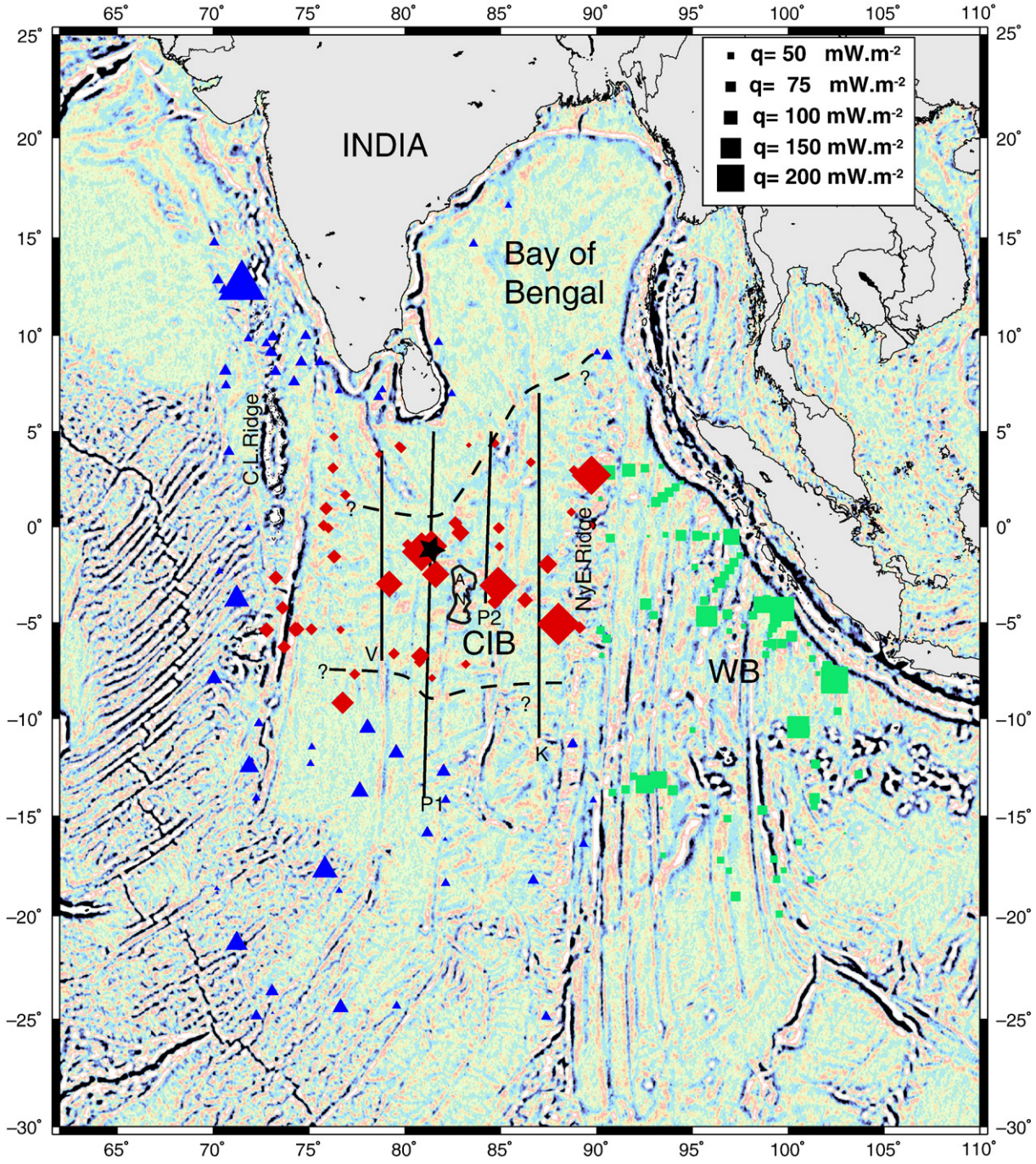

Fig. 1. Location of surface heat-flow measurements in the Indian Ocean and some of the seismic tracks where E–W thrust faults have been imaged. V: Conrad monotrace profile (VanOrman et al., 1995); P1: Phèdre Leg1 wide angle profile; P2: Phèdre Leg2 wide angle profile (Chamot-Rooke et al., 1993); K: Eastern CIB seismic profile (Krishna et al., 2001). Red symbols cover the Central Indian Basin, green symbols the Wharton Basin, blue symbols the remaining areas. The size of the symbol is proportional to the heat-flow value. Background is a filtered Sandwell 15.1 satellite (Sandwell and Smith, 1997) gravity field showing contrasting structural trends on both sides of NinetyEast Ridge. Contour of the Afanasy Nikitin Seamount is also shown. The ODP Leg 116 site is represented by a star. (For interpretation of the references to color in this figure legend, the reader is referred to the web version of this article.)

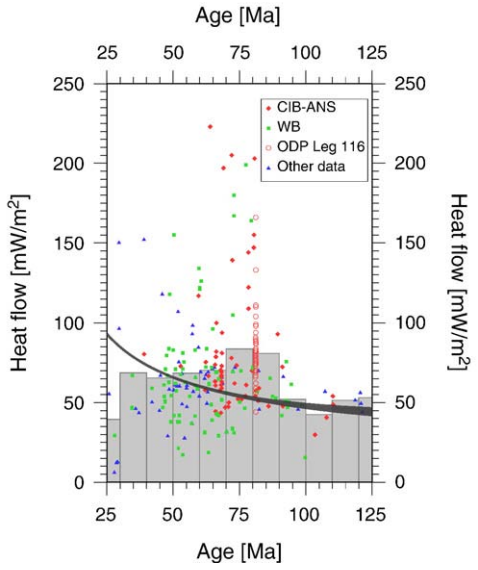

Fig. 2. Surface heat flow versus age of the oceanic lithosphere in the Indian Ocean. Colors and symbols are similar to Fig. 1. A 10 Myr binning is superimposed, as well as two conductive plate models (dark envelope) for two different plate thickness (95 km and 125 km). CIB: Central Indian Basin; ANS: Afanasy Nikitin Seamount; WB: Wharton Basin.

mantle reflectors that do not seem to connect to active faults were also found. Brightness of the fault planes was further interpreted as evidences for water circulation (Bull and Scrutton, 1990b).

Discarding the possibility of a pre-deformation large-scale reheating due to external sources, we quantitatively examine in this paper two heating mechanisms that may explain the strong link between fault localization and high heat flow: friction on the thrust fault network and exothermic serpentinization. Our analysis is based on reprocessed multichannel seismic data showing new evidences for fluid paths down to the mantle and associated enigmatic deep, bright reflectors. We successively discuss evidences for serpentinization in the Indian Ocean, the role of fluid convection, expansion during serpentinization and finally other sites of serpentinization in the oceans.

2. Data

2.1. Heat flow versus age analysis

The global heat-flow compilation by Pollack et al. (1993) includes some 300 measurements acquired in the Indian Ocean during various surveys since the 1960's, to which we have added measurements from the pre-site survey of ODP Leg 116 drilling (Cochran et al., 1989) (Fig. 1). Heat-flow values range from 2 mW/m^2 to more than 200 mW/m^2. We show in Fig. 2 the distribution of heat flow as a function of age of the underlying oceanic lithosphere. The main figure is not different from what was published previously (e.g. Geller et al., 1983; Stein and Weissel, 1990) but we choose to split the data into three subsets: the Central Indian Basin (including the region of the Afanasy Nikitin Seamount Chain), the Wharton Basin, and the remaining data. The first two subsets cover areas that are presently suffering active deformation. Theoretical plate cooling models are given for comparison. Quality of data was

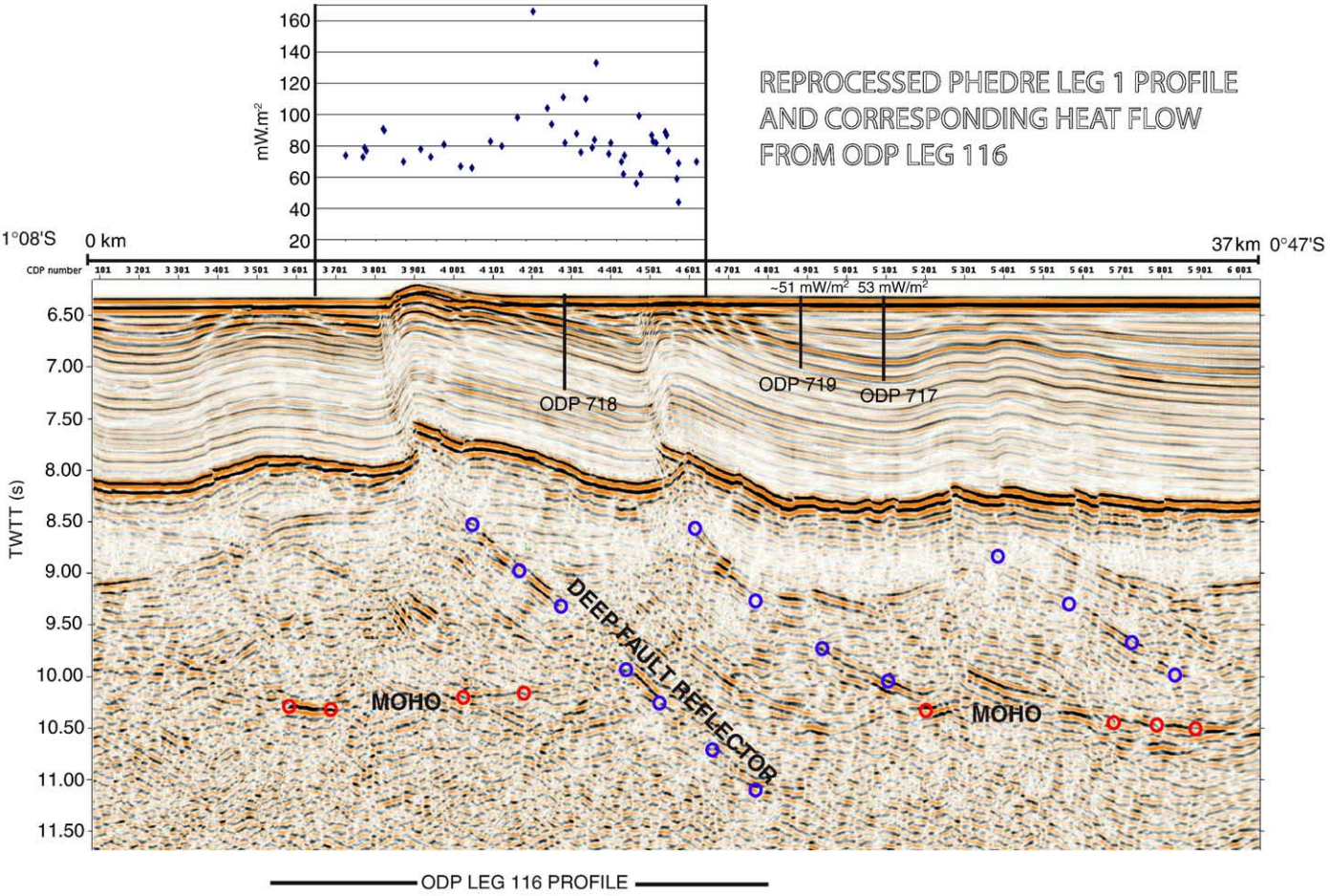

Fig. 3. Portion of the reprocessed multichannel Phèdre line across the ODP Leg 116 site. Top inset shows the detailed heat-flow measurements obtained above two active faults during the ODP Leg 116 pre-site survey (Shipboard Scientific Party, 1989). Open dots underline deep crustal and mantle reflectors.

discussed in a number of papers and they all concluded that the heat flow was abnormally high (Geller et al., 1983; Stein et al., 1988; Stein and Weissel, 1990; Williams, 1990; Ormond et al., 1995).

The observed heat flow is widely scattered above and below the plate cooling model predictions. This type of scattering may be the result of transient hydrothermal circulations, and indeed some of the temperature gradients were demonstrated to be non-linear (Geller et al., 1983). An over simplistic view is that the lowest heat-flow values are sites of recharge of cold fluids whereas highest heat-flow values are hot fluids seeping sites. However, the Central Indian Basin definitely shows a different pattern, the mean heat flow there being clearly above the theoretical predictions. An alternative to the high heat-flow anomaly interpretation is that the measurements systematically "missed" the recharge areas, as suggested by apparently normal values estimated within two ODP holes (Williams, 1990). This alternative interpretation was dismissed in Stein and Weissel (1990) and Ormond et al. (1995), as will be discussed in a latter section.

The high heat-flow anomaly appears to be restricted to the Central Indian Basin, since the Wharton Basin seems to show the right thermal age (Stein et al., 1988). Actually, the Cretaceous Central Indian Basin (mean age of 74 Ma at measurements sites) has a higher surface heat flow (80 mW/m^2) than the younger Wharton Basin (mean age of 61 Ma and average heat flow of 65 mW/m^2). The simplest interpretation is that in the Central Indian Basin, convective hydrothermal circulation is superimposed onto an abnormally hot conductive lithosphere, and that both processes are intimately linked to the active fault network. Hydrothermal circulation may also be present in the Wharton Basin, but the background heat flow there is presently normal.

2.2. Spatial correlation between high heat flow, high straining regions and active faults

Seismic profiling allows us today to draw a quite accurate contour of the thrust fault network in the Central Indian Basin. It spreads along a roughly equatorial zone around the Afanasy Nikitin seamount, from 70°E to the NinetyEast Ridge and from 7°S to approximately 5°N. At large scale, the high heat-flow values cover more or less the thrust fault network. In our recent kinematic study of India–Australia intraplate deformation (Delescluse and Chamot-Rooke, 2007), we showed that the best instantaneous strain rate field, in terms of style and amplitude of deformation, is obtained when heat flow is used as a proxy for rheological strength of the Indian Ocean oceanic lithosphere. In the northeastern Indian Ocean, this is equivalent to considering the entire fault network area as weak.

At shorter scale, best evidences for correlation between high heat-flow and active deformation come from one detailed heat-flow profile across the ODP Leg 116 site (Fig. 3). This ~15 km-long profile was sampled every half a kilometer or less. The 44 heat-flow measurements average 84 mW/m^2, with a peak value at 166 mW/m^2 between two active reverse faults both with large offsets. A reprocessed multichannel line of the Phèdre Cruise over the same area (Fig. 3) shows that the fault reflectors plunge deep into the mantle, below Moho seismic phases. At the scale of these two faults, the heat-flow profile thus reproduces the Central Indian Basin large-scale anomaly of 25–30 mW/m^2. Ormond et al. (1995) successfully modeled the bell shape of the heat-flow anomaly assuming vigorous fluid circulation within the fault planes above an abnormally hot basement. Williams (1990) also proposed a set of models in which faults are included as conduits.

These elements suggest that the spatial correlation – both global and local – between faulted seafloor and thermal anomaly is not a coincidence. The question that arises is whether the present-day deformation is a cause or a consequence of the thermal anomaly. That phase of deformation began 7.5 (Cochran et al., 1989) to 9 (Delescluse et al., 2008) Myr ago as documented by regional late Miocene unconformities in the Indian Ocean sediments. Stein et al. (1988) noticed that there was no clear correlation between the exact location of the earthquakes and the high heat-flow sites, probably because of the large uncertainties on the position of the epicenters. Nevertheless, they suggested that the absence of heat-flow anomaly and the low seismicity in the Wharton Basin was indicating that it is presently deforming much less than the Central Indian Basin. We know today that the seismicity is not that low in the Wharton Basin (i.e. Mw = 7.9, 2000; Mw = 6.9, 1995) and that the strike-slip motion accommodated there is significant (Deplus et al., 1998). Summing moment tensors of earthquakes, we actually found that the Wharton Basin is presently the highest straining region of the Indian Ocean (Delescluse and Chamot-Rooke, 2007). Strain is thus highest in a region where heat flow is close to normal, which seems paradoxical both if heating is the cause or the consequence of the deformation. WB and CIB areas are actively deforming, but with contrasting style of faulting: mainly E–W reverse faults in the CIB and sinistral shear on N–S vertical faults in the Wharton Basin (Delescluse and Chamot-Rooke, 2007) (Fig. 1). We will show in a latter section that the contrasting heat-flow anomaly between the two regions is indirectly related to this contrasting style of deformation.

3. Origin of the heat source

We review here two different mechanisms that have been proposed as potential heat sources for the Central Indian Basin. Both are tectonically driven: friction-to-heat conversion on the thrust fault network and exothermic serpentinization along the fault planes at mantle depth. We do not take into account the possibility of a hot-spot reheating of lithosphere here, as it has already clearly been discarded in Stein and Weissel (1990).

3.1. Friction on faults

Shear friction on faults has long been recognized as a potential source of heat, in particular at large continental strike-slip faults (Lachenbruch and Sass, 1980; Scholz, 2000; D'Alessio et al., 2006) and at subduction zones (Wang et al., 1995). Crude estimations have been proposed for the reverse faults of the Indian Ocean (Geller et al., 1983), but we now have a much more detailed picture of the thrust network, including fault spacing, geometry of the faults at depth, rate of deformation. 134 reverse faults were recognized along one Phèdre deep seismic profile that span the entire region of deformation in the Central Indian Basin, 30% of them associated with fault reflectors within the crust itself with an average dip angle of 36° to 45° (Chamot-Rooke et al., 1993; Jestin, 1994). Two of these reflectors are clearly imaged in the region of the ODP Leg 116 site (Bull and Scrutton, 1990a), and our reprocessing shows that they cut through the entire crust, intersect the Moho discontinuity and plunge deep into the upper mantle.

Our calculation of the friction-related anomaly is based on the diffusion of heat in a half-space (Carslaw and Jaeger, 1959) adapted by Lachenbruch and Sass (1980, 1992) for the San-Andreas strike-slip fault. The rationale is to sum the individual contribution of each fault along the entire profile length. Shear heat flow along a profile normal to a vertical fault plane is:

$$q(y,t) = \frac{Q_c}{2\pi}\left[E_i\left(-\frac{x_2^2+y^2}{4Kt}\right) - E_i\left(-\frac{x_1^2+y^2}{4Kt}\right)\right] \quad (1)$$

where y is the horizontal distance to the surface fault trace, t is time, x_1 and x_2 are the minimum and maximum depth of the brittle portion of the fault, Q_c is the product of the depth-averaged shear stress by the fault slip-rate, E_i is the exponential integral function, K is the thermal diffusivity.

This formalism is readily adaptable to a thrust fault with a dip angle θ. This is done by the discrete summation of infinitesimal vertical planes disposed every dx depth unit along the fault plane with length of $\frac{dx}{\sin(\theta)}$ to keep the size of the frictional surface identical. This

also allows for variable shear stress with depth. The heat-flow anomaly across one thrust fault is then:

$$q_1(y,t) = \sum_{j=0}^{\left[\frac{x_2-x_1}{dx}\right]} \frac{Q(x_2-jdx)}{2\pi} \left[E_i(R_{j2}) - E_i(R_{j1})\right] \quad (2)$$

where R_{j1} and R_{j2} are functions of distance from the calculation point (x=0,y) to respectively the top and bottom of each infinitesimal vertical plane. $Q(x) = \frac{V}{\cos(\theta)} \cdot \tau_s\left(\tau_s = \frac{\mu\rho g x}{1-\mu\tan(\theta)}\right)$ is now the product of the shear stress – at depth x on the thrust fault plane of dip θ – by the fault slip-rate. Although these equations are strictly valid for infinitely long fault, which is obviously not the case in the Indian Ocean, they still provide a reasonable estimation of the heat input since the fault network extends for nearly 2000 km in the EW direction, much larger than the typical depth of the faults.

The final thermal anomaly is obtained by summing the effects of faults spaced at regular intervals to simplify the natural situation. All calculations were performed using a shortening rate of 1 cm/yr integrated along the entire length of the profile crossing the fault network, which can be regarded as an upper limit (Chamot-Rooke et al., 1993; Delescluse and Chamot-Rooke, 2007). For simplicity, all faults dip in the same direction, based on the observation that very large portion of the deformed oceanic crust (100–200 km) actually show uniform fault dips (Jestin, 1994). The depth of the brittle lithosphere is chosen to be 40 km, based on the maximum depth of earthquakes in the area (Stein and Weissel, 1990). The shear stress follows a standard Byerlee's law with null pore fluid pressure, which again will tend to overestimate the frictional heat due to unrealistic high shear stress at depth. A standard faults spacing of 7 km was used, but larger spacing was also tested since large offset faults are rather 20–30 km spaced. The period of activity is set to 7.5 Myr.

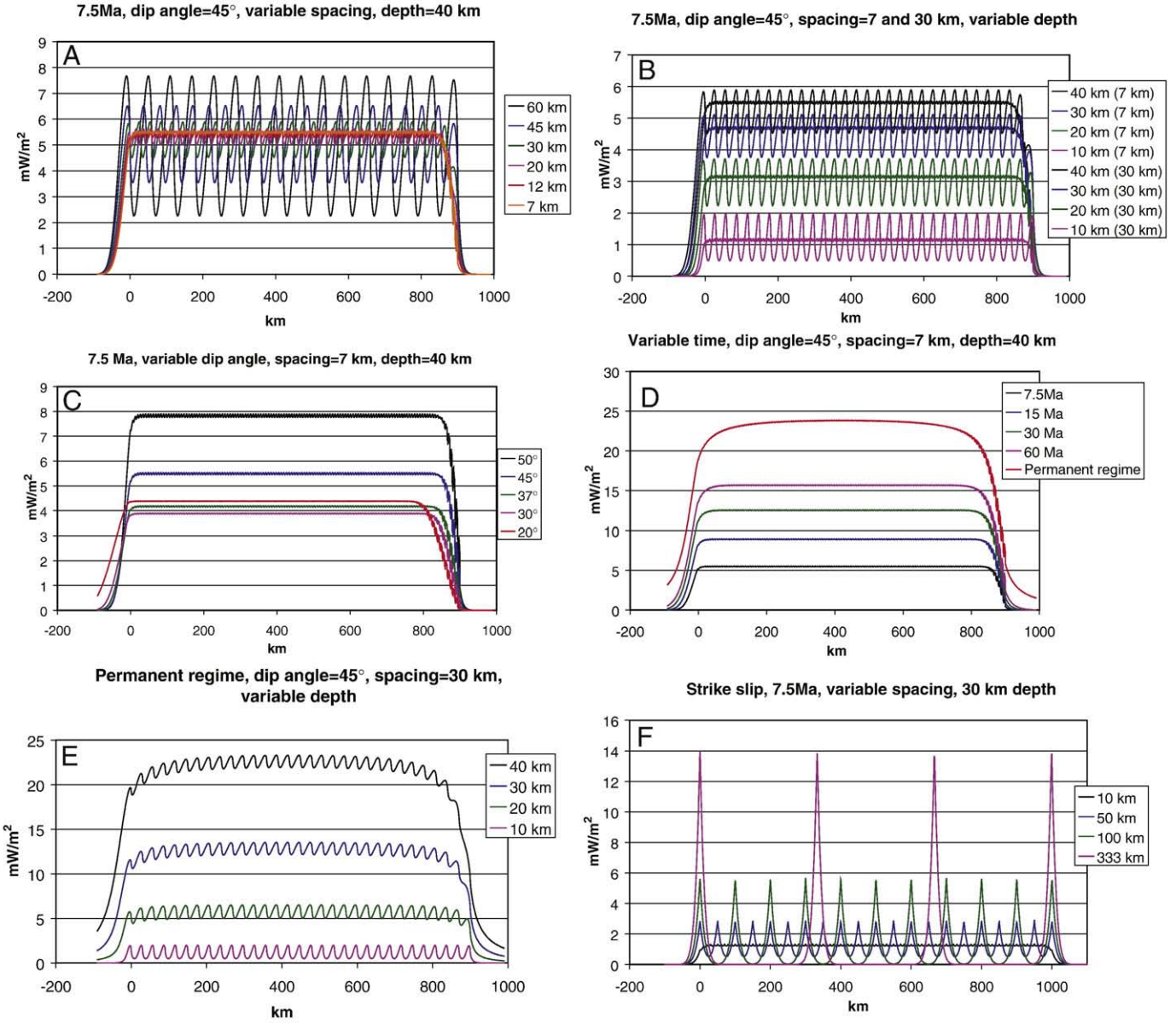

Fig. 4. Main results of the friction heat production model. All graphs are transient states 7.5 Myr after the onset of deformation, except Graph D (gives the thermal evolution through time) and E (reaches permanent regime). Graphs A to E are 900 km-long profiles across the reverse faults network (Central Indian Basin model, 1 cm/yr of total shortening). Graph F is a 1000 km crossing vertical strike-slip faults (Wharton Basin model, 2 cm/yr of total shearing). A) Faults spacing variation; B) Brittle depth variation; C) Dip-angle variation; D) Evolution through time; E) Brittle depth variation (permanent regime); F) Strike-slip faults spacing variation.

Fig. 4 shows the sensibility of the frictional model to some of the main parameters. Varying the fault spacing (Graph A) does not change the overall level of the thermal anomaly (~5.5 mW/m^2) since the integrated amount of shortening remains identical. Given the overestimation that we made, it is readily apparent that friction cannot explain the observed heat-flow anomaly.

Some other straightforward and useful information can be extracted from the model. Shearing on individual faults could eventually be detected through surface heat-flow measurements if their spacing would be greater than 40 km (Graph A). By varying the thickness of the brittle zone (Graph B), we learn that the heat source must be shallower than 10 km to clearly individualize 30 km spaced faults: whatever the strength and mechanism, if the heat source is linked to the faults, heat conduction implies that we have virtually no chance – given the number of faults – to measure a non-anomalous heat flow.

The lower the dip angle, the greater the frictional surface. However, this effect is over compensated (Graph C) by the fact that the slip-rate grows for larger dip angles, and also that the shear stress grows when the dip angle is larger than $\frac{\pi}{4}-\frac{1}{2}a\tan(\mu)$. This is however not sufficient to reach heat-flow anomalies significantly greater than 5 mW/m^2. The next graphs show the evolution through time before permanent regime is reached. A period of 7.5 Myr of heating is far from the permanent regime if the source is deep (40 km in Graph D). A permanent regime is almost reached if the source depth is shallower than 10 km (compare Graph E and Graph B), but then the thermal anomaly is small.

We performed the same calculations for the Wharton Basin to evaluate frictional heating along a 1000 km-long E–W profile normal to the active N–S strike-slip faults (Graph F). The total rate of shear was assumed to be 2 cm/yr, which is probably maximized (Delescluse and Chamot-Rooke, 2007). Our calculations lead to a maximum heat-flow anomaly ranging from a ~1 mW/m^2 1000 km-long plateau – in the case of 10 km spaced strike slip faults – to narrow 14 mW/m^2 spikes if the shear is distributed onto 4 faults only. If shear heating is present in the Wharton Basin, the chance to resolve it with surface heat-flow survey is low unless measurements are performed close to the reactivated fracture zones.

3.2. Exothermic serpentinization

Some serpentinization reactions are known to be significantly exothermic (Fyfe, 1974; Lowell and Rona, 2002; Fruh-Green et al., 2003; Emmanuel and Berkowitz, 2006). Such heating seems to play a major role in the Lost-City vent field near the Mid Atlantic Ridge, where mantle peridotites are exhumed at shallow depth (Fruh-Green et al., 2003). It may be held responsible for sustained convection in this off-ridge area (Kelley et al., 2001; Lowell and Rona, 2002; Emmanuel and Berkowitz, 2006). Exothermic serpentinization is thus an appealing mechanism to generate heat at rather shallow depth, and we will review pieces of evidence that it may be at work in the Indian Ocean in Section 4. Beyond the crude estimates found in Verzhbitsky and Lobkovsky (1993), we describe here the thermal model that we built to quantitatively calculate the amount of heat that may be available in the deforming portion of the Indian Ocean.

3.2.1. Thermal model and kinetics of the serpentinization reaction

The hydration reaction is possible up to temperatures of 400 °C (Emmanuel and Berkowitz, 2006) to 500 °C (Francis, 1981). The reaction is most efficient around 250–300 °C (MacDonald and Fyfe, 1985; Fruh-Green et al., 2003; Emmanuel and Berkowitz, 2006) where lizardite is the stable mineral while greater temperatures and pressures lead to a stable antigorite mineral (Christensen, 2004). The reaction becomes extremely slow around and below 100 °C. The typical rock temperature at Moho depth is ~120 °C for a Cretaceous oceanic lithosphere, which potentially allows for serpentinization in the lower oceanic crust and in the upper mantle down to ~25 km. We consider that the mantle is virtually anhydrous at these depths in the Central Indian Basin, since any serpentinization process that would have occur at the very early formation of the oceanic lithosphere would have been active at shallow levels only due to the high thermal state at the ridge axis.

We use here the reaction kinetics described in Emmanuel and Berkowitz (2006), i.e.:

$$\frac{\partial \rho_f}{\partial t} = -K_r \rho_f \tag{3}$$

where ρ_f is the volumic mass of forsterite in the mantle. K_r is the rate coefficient, expressed as $K_r = Ae^{-b(T-c)^2}$, this last formulation being empirically constructed from kinetic data (Emmanuel and Berkowitz, 2006). A, b and c are different kinetic coefficients compiled in Table 1. Serpentinization produces H=290 kJ/kg of forsterite (MacDonald and Fyfe, 1985; Emmanuel and Berkowitz, 2006).

We also use the rate of heat generation per unit volume defined in Emmanuel and Berkowitz (2006) as:

$$Q = H \cdot \frac{\partial \rho_f}{\partial t}. \tag{4}$$

We finally assume that there is 75% of forsterite in the mantle which leads to $\rho_f(t=0)$=2400 kg m^{-3} for a mantle density of ρ_m=3200 kg m^{-3}.

A 2D finite difference algorithm is used to solve the transient heat diffusion equation with spatially and temporally variable heat production. We do not take into account volume changes for simplification, but we will discuss the matter in Section 4. Simple lithosphere cooling is first solved in 1D until t_{start}=72.5 Ma, which will represent the approximative thermal state at the onset of deformation (~56 mW/m^2). The 2D finite difference grid is then chosen to be 30 km wide and 125 km deep with a cell dimension of about 150 m × 150 m. 45° dipping faults are disposed regularly, with periodic thermal boundary condition, which is a good way to get rid of side effects, and is appropriate for the fault network that we study. Heat production then follows serpentinization fronts moving horizontally away from the fault planes (Fig. 5). The reaction in the heating fronts is forced to stop when half of the forsterite is serpentinized. At time t_{stop}=80 Ma, we thus obtain an average 50% serpentinization which leads to a density of ~2900 kg m^{-3}. The rationale is to keep the mantle density close to the value obtained by Louden (1995) at the base of the crust.

The amount of heat produced and the temperature field evolution through time are mainly controlled by three parameters: (1) the reaction rate coefficient A, which is a measure of the efficiency of the serpentinization reaction; (2) the serpentinization front velocity S, which will relate to the mechanical strength around the fault; and (3) the fault spacing, i.e. the initial surface of serpentinization. Fault spacing was set to 10 km in most of the runs, which is the distance between the main faults observed at the ODP Leg 116 site. The first two parameters are very difficult to set in a deep environment. One of the rare studies dealing with serpentinization in relatively deep (5 km) oceanic environment (MacDonald and Fyfe, 1985) quotes velocity of 1000 m/Myr at 300 °C for water propagation in the host rock from an open crack. The same value is used by Ranero et al. (2003) for serpentinization that may be active around the bending related normal faults at subduction bulges.

The kinetics of the serpentinization is even less constrained. It is fast when operated in the laboratory (a few days, $A \simeq 10^{-6}$ s^{-1}), but it is most probably much slower in situ because of a smaller reaction surface (Emmanuel and Berkowitz, 2006). An additional limiting factor is the water supply (MacDonald and Fyfe, 1985) rather than the kinetics

Table 1
Parameters for the kinetics of serpentinization

Rate coefficient magnitude	A	0.5 to 8 × 10^{-12} s^{-1}
Peak reaction temperature	c	540 K
Kinetic coefficient	b	2.5 × 10^{-4} K^{-2}
Serpentinization front velocity	S	300–2000 m/Myr

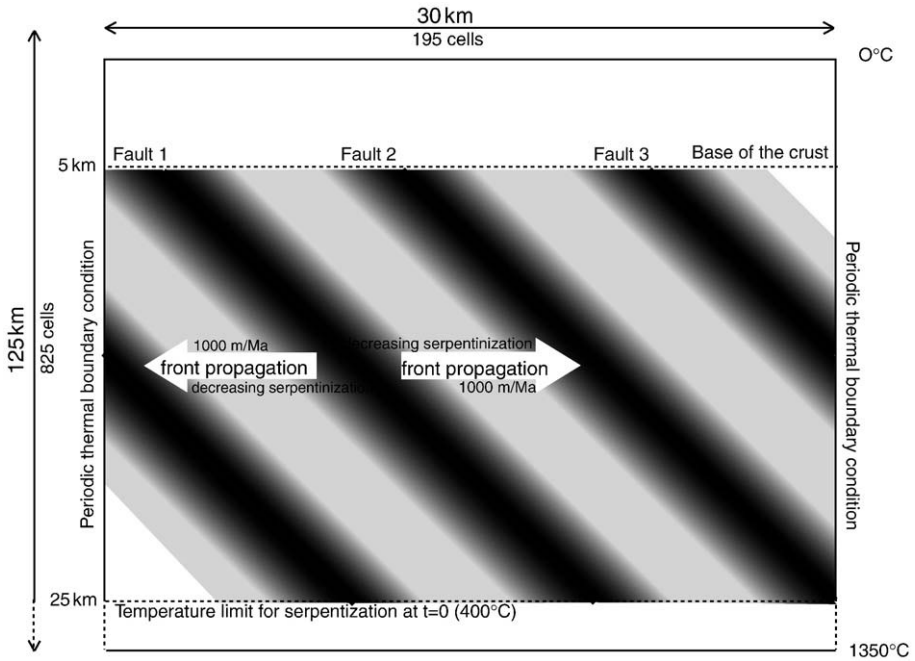

Fig. 5. Sketch for the serpentinization model. Serpentinization fronts propagate horizontally from the faults; Serpentinization ends in cells where 400 °C is reached. Periodic thermal boundary conditions are assumed on both sides. Grey shading indicates the degree of serpentinization.

itself. We choose a rate coefficient magnitude (A) spanning two orders of magnitude and somewhat smaller than what is used by Emmanuel and Berkowitz (2006) (i.e. around 10^{-12} s^{-1} instead of $\sim 10^{-10}$ s^{-1}), assuming that the reaction surface at depth is less compared to the shallow environment of Lost-City. Half-life of the reaction is then around 20,000 yrs at peak temperature, the coefficient b being chosen so that the reaction is extremely slow for temperatures below 100 °C and also virtually stopped above 400 °C (Emmanuel and Berkowitz, 2006).

3.2.2. Results of the serpentinization model

The goal is to reach at least a 20 mW/m^2 surface heat-flow anomaly, which would be a significant part of what is observed today. The second constraint is timing, since a fundamental difference of the serpentinization model compared to the frictional heating model is that the source decays with time: by essence, the obtained anomaly is thus transient and vanishes with time. Fig. 6 shows one typical run and summarizes the sensitivity of the results to the main parameters. The test run is for a 10 km faults spacing and a typical front velocity of 1000 m/Myr. The associated temperature anomaly in the upper mantle does not exceed 80 K and lasts a few Myr only. In the case of a shorter fault spacing, not shown here, the temperature field is more homogeneous and does not exceed 50 K. In all cases, the temperature anomaly is limited to depths between 5 and 25 km. A low temperature anomaly and a thermally quasi-normal lithosphere were actually two requirements quoted in the early study of Stein and Weissel (1990).

In this simple test run, the peak surface anomaly (22 mW/m^2) is reached about 5 Myr after the onset of serpentinization and remains above 10 mW/m^2 the remaining 2 to 3 Myr. Faster front propagation (S=2000 m/Myr) produces a sharper peak anomaly of 30 mW/m^2 which does not last long enough, while slow propagation (S=500 m/Myr) just reaches a low maximum of ~12 mW/m^2 at 80 Ma. Changing the kinetics results in marginal variations: increasing A to $\sim 10^{-11}$ s^{-1} does not produce a higher heat flow for any of the assumed front velocities. The reason is that faster reaction rates result in a saturated heat output, since the velocity of the serpentinization front is the true limiting factor. When the front propagates to the next discrete 150 m wide cell of the model, the previously hydrated volume has already released all of its potential heat. In other words, in our model, the reaction is water limited, and is equivalent to the successive serpentinization of spatially limited massifs modeled – or idealized – by the serpentinization front. Finally, decreasing the fault spacing to 7.5 km or even to 3 km has little effects, provided that the front propagation velocity is downgraded (respectively to S=750 m/Myr and S=300 m/Myr). This is not surprising, since a constant fault spacing to front propagation ratio results in a similar history of serpentinization (i.e. 50% serpentinization completed after 5 Myr).

Several sets of parameters thus lead to the required surface heat flow. The remaining difficulty is that the peak anomaly generally comes too early in the thermal history. One possibility is that serpentinization was delayed with respect to the initiation of deformation. In the 3 km spaced faults case, a linear progression of the serpentinization front velocity from 150 m/Myr to 500 m/Myr would correspond to an onset of serpentinization at 6.25 Ma. Equivalent scenarios can be reached with 7.5 km and 10 km faults spacings (Fig. 6, C-curves 1). New seismic data published in Delescluse et al. (2008) show massive reactivation of the 3 km spaced oceanic fabric normal faults at 9 Ma. After a 2 Myr period, faults are selectively abandoned and only the present-day active faults remain. Our model is thus in better agreement with the onset of this second phase of deformation starting at 7 Ma under the effect of a severe weakening of fault planes Delescluse et al. (2008).

4. Discussion

4.1. Clues to serpentinization in the CIB

Arguments in favor of past and present serpentinization in the Indian Ocean mainly come from various seismic data. Refraction data in the CIB southwest of the ODP site revealed a low velocity zone in the lower crust, interpreted as partially serpentinized (~35%, ρ=2950 kg/m^3) clasts of peridotites in the gabbro Louden (1995). One seismic reflection profile shows injection into one reverse fault that has been interpreted as a serpentinite diapir based on gravity modeling (Krishna et al., 2002). Seismic refraction data from Russian surveys also

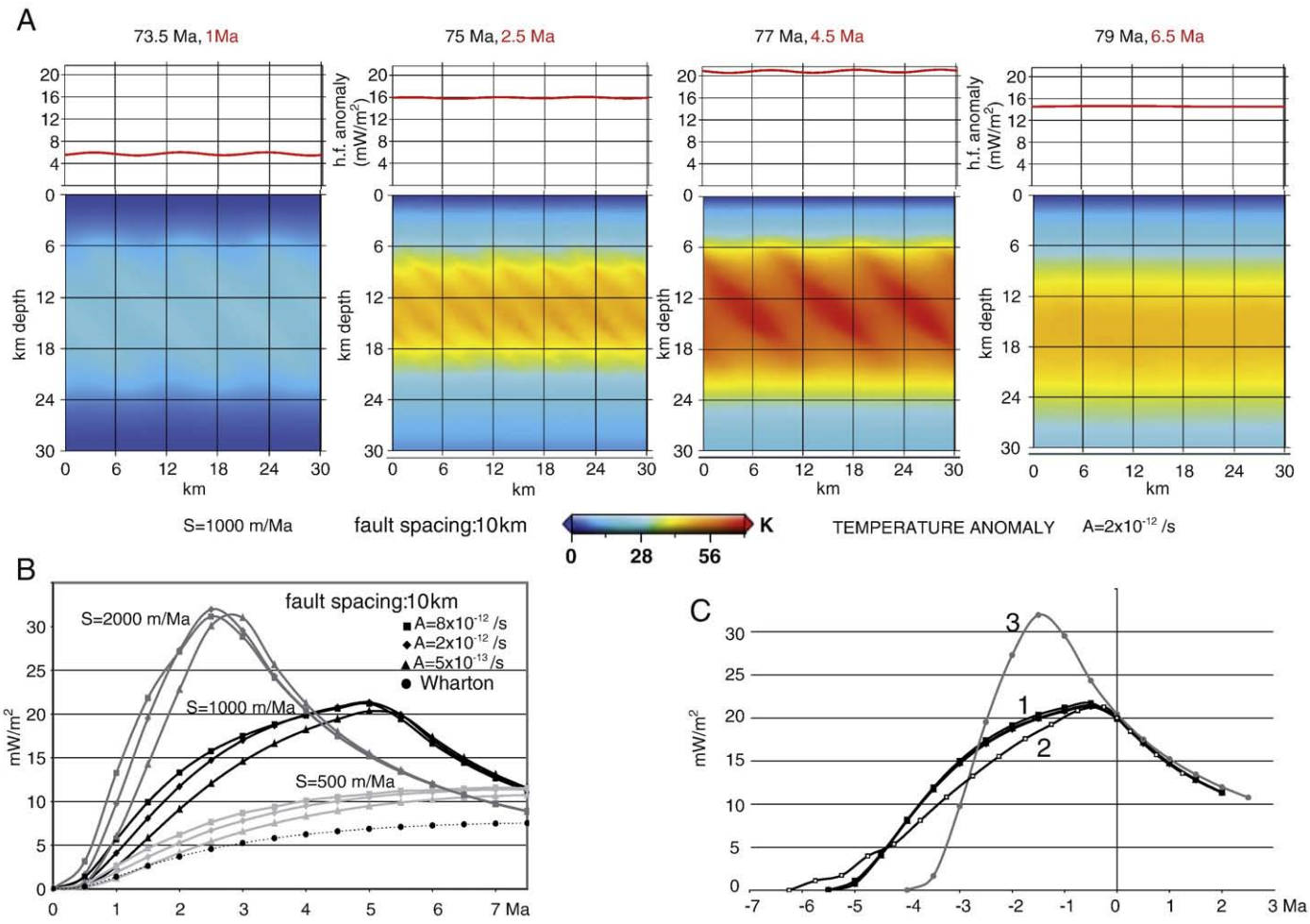

Fig. 6. A) Snapshots of the anomalous thermal field through time for the exothermic serpentinization model after 1 Myr, 2.5 Myr, 4.5 Myr and 6.5 Myr of deformation; B) Evolution of the surface heat flow through time since the onset of deformation for three different serpentinization front velocities (500, 1000 and 2000 m/Myr) and variable kinetic coefficients. Dotted curve is for Wharton Basin with vertical faults having 30 km spacing and a serpentinization front velocity of 1000 m/Myr. C) Evolution of the surface heat flow with the *x* axis chosen so that all models still reach 20 mW/m^2 at the origin: 1) Three overlapping curves show equivalent thermal history for different fault spacings (10 km, 7.5 km, and 3 km) but scaled serpentinization front speeds (respectively 1000 m/Myr, 750 m/Myr and 300 m/Myr); 2) Test for a linearly increasing serpentinization front velocity with time (from 100 m/Myr to 500 m/Myr with 3 km fault-spacing); 3) Test for a high serpentinization front velocity 2000 m/Myr for comparison.

suggest velocities up to 7.3 km/s in the shallow crust, which could be related to such diapirism (MacDonald and Fyfe, 1985; Levchenko and Verzhbitsky, 2003; Verzhbitsky and Neprochnov, 2005).

We provide new pieces of evidence from our reprocessing of one Phèdre seismic profile, where we detect enigmatic, bright and oblique reflectors deep in the mantle (Fig. 7). These reflectors are disposed at the termination of a much less visible reflector which connects at the basement interface with a clear reverse fault. Their approximate depth (8 to 15 km) coincides with the maximum value of the serpentinization reaction rate. We thus interpret these very bright reflectors as serpentinization fronts – either active or fossil – near an active thrust fault used as fluid path. Deeper reflectors may be present, since the serpentinization rate drops 20 km below the top of crust (Figs. 6,7). Finally, serpentinization of peridotites appears as a quite efficient heating mechanism: the transient heat-flow anomaly it produces is much larger than what friction can provide (~20 mW/m^2 versus ~5 mW/m^2), recalling that we maximized the friction effect in our calculations. However, extreme surface heat-flow values cannot be modeled without including fluid flow: the exothermic serpentinization provides a strong enough basal heat flow at depth, which is then redistributed by convective fluid circulation in the sediments (Ormond et al., 1995), but also possibly in the crust (Louden, 1995). Our thermal model shows that serpentinization is compatible with a wide range of present-day surface heat flow (including close to normal values), taking into account the transient nature of the thermal anomaly. Serpentinization requires a significant fluid input that we did not discuss nor take into account in our conductive model. The question of the long term access of fluids to fresh mantle also has to be addressed.

4.2. Downward flow of water required by serpentinization: amount and thermal effect

First, the required water input rate is not unrealistic. Serpentinization consumes 300 L of water per cubic meter of olivine (MacDonald and Fyfe, 1985; Fruh-Green et al., 2003). Our model involves half serpentinization of, say 20 km (depth)×30 km (width)×1 km (arbitrary since our model is 2D)=600 km^3 of olivine, which means that we have to bring a total of $0.5\times600\times300\times10^9=10^{14}$ L of water during the 5 Myr reaction period. This is equivalent to a flow of ~0.02 μL s^{-1}.m^{-2}, or 0.6 L s^{-1} through the 30 km×1 km arbitrary surface at the seafloor. With a conservative value of one single fault used as fluid path every 30 km, and a fluid path width of 10 m, the downward fluid velocity is around 6×10^{-8} m s^{-1}. This value is similar to the 7×10^{-8} m s^{-1} upward fluid velocity derived from non-linear temperature gradients by (Geller et al., 1983).

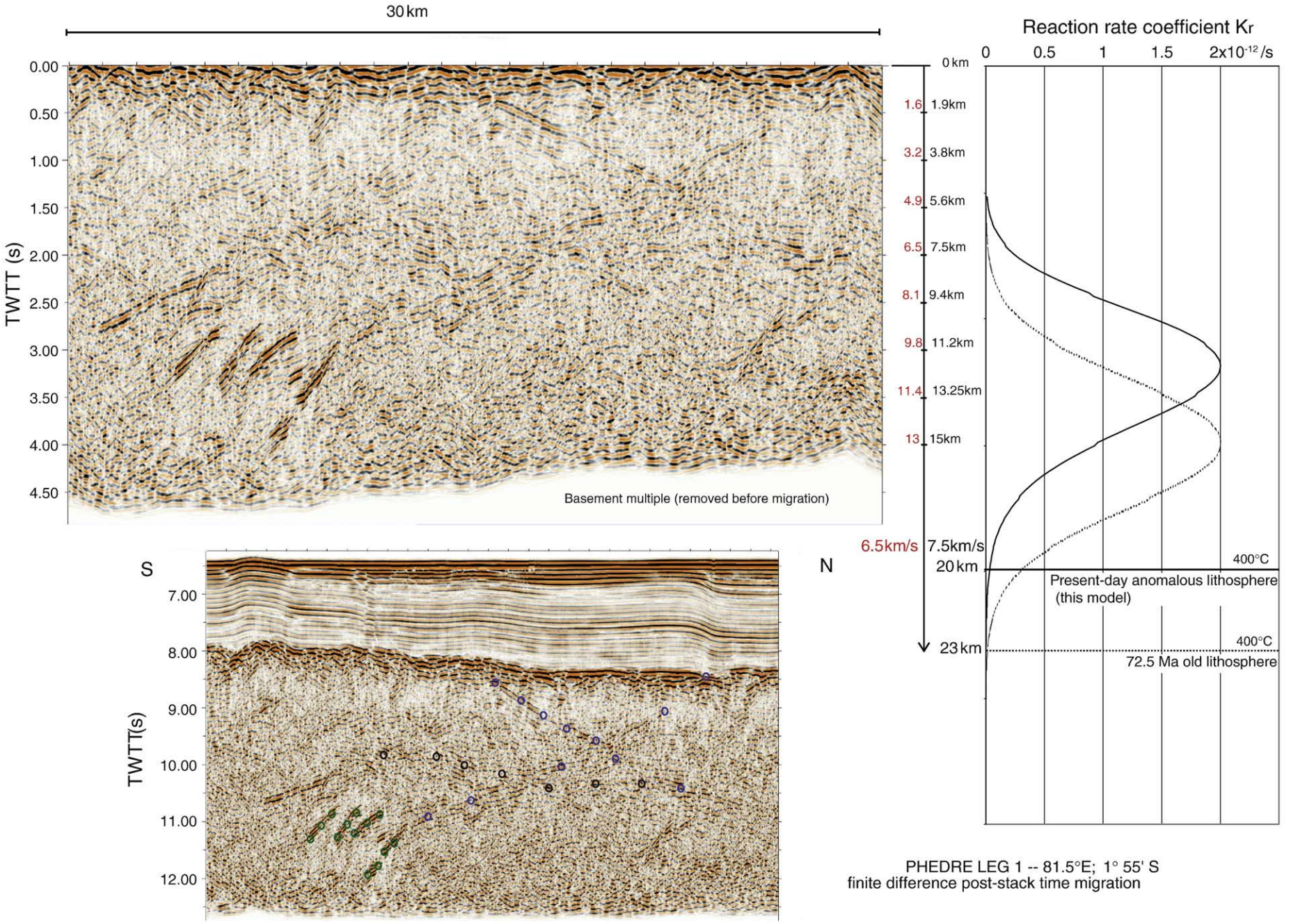

Fig. 7. Bottom: Phèdre Leg 1 reprocessed profile showing deep and bright reflectors at sub-Moho depth. Top: Same profile with sediments removed, using trace time-shift and mute to start the display at the top of the oceanic crust. The two-way travel time is converted to depth using two different values for the mean velocity (6.5 km/s and 7.5 km/s). Right: Reaction rate coefficient for serpentinization as a function of depth, at the time of initiation of deformation and 7.5 Myr later. Bright enigmatic reflectors coincide with the predicted depth of maximum rate of serpentinization and are interpreted as serpentinization fronts.

The nature and extent of recharge zones are however unknown and the calculated velocity above is likely to be overestimated. The search for fluid recharge zones was central to the debate on the ODP Leg 116 heat-flow profile interpretation due to the absence of lower than normal heat-flow measurements in the CIB. Williams (1990) proposed a fluid advection process to explain the 84 mW m^{-2} average value, the modeled section (15 km) being considered as a discharge zone. No additional heat source is necessary but this approach requires a distant recharge zone where downward flow of water should cool the sediments. Such a zone where the heat flow would be lower than normal has never been observed. The probability that all measurements missed recharge zones is small, and this leaded previous authors (Geller et al., 1983; Stein and Weissel, 1990; Ormond et al., 1995) to conclude to an anomalously hot basement. Ormond et al. (1995) set up a 3D model including anomalous basal heat flow, and showed that fluids are more likely to convect in the fault planes themselves rather than between two faults through a deep conduit. In this case, along-strike variations of heat flow should be observed and recharge zones are those where heat flow equal the theoretical values. Although we cannot totally rule out that the linear temperature gradients at ODP sites 717 and 719 showing normal heat flow (Fig. 3) do represent the conductive background heat flow, they may equally be these areas of diffuse recharge.

If exothermic serpentinization is responsible for the high heat-flow anomaly, then the required deep downward flow of water (i.e. water needed to feed the serpentinization reaction) must be negligible compared to the surface fluid convection input, otherwise low heat-flow values should be observed. Ormond et al. need 2×10^8 L $yr^{-1}.km^{-2}$ of water input in their model while serpentinization only needs $\sim 2\times10^7$ L $yr^{-1}/(30\ km^2)=7\times10^5$ L $yr^{-1}.km^{-2}$, which is more than two orders of magnitude less. We thus conclude that the deep downward flow of water probably has a limited cooling effect if recharge zones are diffuse.

4.3. Water progression in the oceanic mantle

Serpentinization tends to reduce rock porosity to zero (MacDonald and Fyfe, 1985), so that the fluid paths toward the mantle may become rapidly closed. In a tectonically active setting, the easiest paths for fluids are then faults and cracks, which need to be permanently "refreshed" (Ranero et al., 2003). Our model suggests that a more or less continuous band of serpentinization is needed to reach the required surface heat flow, since isolated massifs of serpentinites would not release enough heat. Connection between propagating serpentinization fronts could be achieved through the dense reverse faults network. The details of the faults population indicate two subsets of faults in the Indian Ocean (Delescluse et al., 2008): (1) small offset faults (<100 m) as close as 2 to 3 km from one another, well expressed in the sediments, in particular on high resolution seismic profiles (VanOrman et al., 1995; Delescluse et al., 2008), and (2) large offset faults, reaching hundreds of meters to a kilometer, generally associated with a deep bright reflector (Chamot-Rooke et al., 1993; Jestin, 1994), with a much larger spacing (about 20 km). If the presence of reflectors is related to water, only the second population of large offset faults could be used as fluid path. Small offset faults are inactive, but they are numerous and the fact that the lithosphere has been highly fractured could help the propagation of water between large faults. Ranero et al. (2003) also notice that some reflectors in the mantle near trench outer rises are not specifically linked to an observed fault at the surface. If as they point in their study, deep reflectors are caused by serpentinization or free fluids, then the 5 to 6 km wide massifs observed in Fig. 7 would suggest that water can propagate several kilometers away from the main fault. The low frequency Phèdre seismic (Ziolkowsky et al., 2003) does not reach the resolution of Ranero et al. seismic, but broadening of faults as they deepen (Ranero et al., 2003) and/or undetected small faults at depth may explain the lateral propagation of fluids.

4.4. Expansion during serpentinization

Expansion during the serpentinization reaction may reach 53% (MacDonald and Fyfe, 1985; O'Hanley, 1992) in volume. On one hand, the difficulty is space accommodation of this additional volume, specifically in a compressional tectonic setting, but on the other hand damages resulting from the volume expansion itself could allow fluid progression. At large degree of serpentinization, expansion should show at the seafloor as uplift, and we should see a shallower than normal seafloor depth. O'Hanley (1992), while acknowledging that field evidences of an increase in volume has not been recognized, mentions that realistic increase in volume is between 25 and 45%. Serpentinization is restricted to a depth of 20 km due to the temperature threshold. 50% serpentinization affecting a 15 km thick column of mantle (with 75% of forsterite) should thus produce a 50%×25%×75%×15,000=1400 m uplift. This is a clear issue of the large-scale serpentinization hypothesis.

The bathymetric anomaly is actually opposite to the one that is predicted by expansion. In details, the unloaded basement depth (Fig. 8) shows that the 300 km buckling wavelength is superimposed on a 800 km-long topographic depression which coincides with the deepest geoid low on earth (Ćadek and Fleitout, 2003; Crosby et al., 2006). This low was interpreted as the dynamic effect of deep mantle sources, such as viscosity variations (Ćadek and Fleitout, 2003). The reference topography in the CIB may thus be significantly deeper than the age prediction. Apart from partially canceling this very long wavelength, the extra volume may also participate to the formation of the buckling wavelength that has grown to a kilometer since the onset of deformation (Gerbault, 2000).

We finally cannot rule out that other hydration reactions are also exothermic. Fyfe (1974) cites some very exothermic hydration reactions in the crust which would double the heat production in our case. Less than 50% of mantle serpentinization would then be needed, leading to a lesser expansion. Unfortunately, we know little about the kinetics of these shallower reactions.

4.5. Serpentinization elsewhere

Fault spacing may explain why, while strain rate is at least as large in the Wharton Basin than in the CIB, no clear heat-flow anomaly is detected there. The two regions exhibit contrasting style of deformation (Deplus et al., 1998; Delescluse and Chamot-Rooke, 2007). The CIB is an area of ubiquitous reactivation of a dense network of normal faults acquired at the ridge axis (Bull and Scrutton, 1990a, 1992; Jestin, 1994; Delescluse et al., 2008), while in the Wharton Basin deformation is

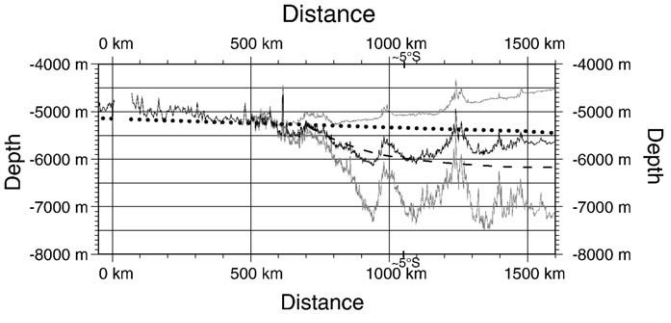

Fig. 8. From top to bottom, bathymetry, unloaded basement depth (black), and basement depth of the entire 1600+ km-long Phèdre Leg 1 seismic profile. The profile starts at 14°S (55 Ma old oceanic lithosphere) and ends around 1°N (90 Ma old oceanic lithosphere). Theoretical basement depth obtained from a plate cooling model is shown by the dotted line (parameters slightly adapted from (Crosby et al., 2006): plate thickness of 95 km and ridge depth at age zero of 2750 m). The dashed line shows a hypothetical reference basement depth in the case of a dynamic topography following the geoidal low of southern India.

accommodated by left-lateral, widely-spaced strike slip faults. Serpentinization may be limited to short distances around them in the absence of a dense active network of secondary faults as found in the CIB. Fig. 6 shows that even if propagation is effective, one vertical fault plane every 30 km leads to a heat-flow anomaly smaller than 10 mW/m^{-2}. One alternative is that heat has already passed in the WB, either because the serpentinization delay may have been shorter or the deformation started earlier there. Mantle dipping reflectors and reduced seismic velocities have been taken as strong evidences for serpentinization of the oceanic mantle at the outer rise of the Middle America Trench, possibly down to 20–30 km (Ranero et al., 2003; Grevemeyer et al., 2007), and at the Central Chile trench outer rise (Grevemeyer et al., 2005; Contreras-Reyes et al., 2007). In both areas, the surface heat flow shows a negative anomaly if any (Grevemeyer et al., 2005). The exothermic nature of the reaction is not discussed and the reduced heat flow is interpreted as the cooling effect of the downward flow of water (Ranero et al., 2003; Grevemeyer et al., 2005; Emmanuel and Berkowitz, 2006) that overcomes the nascent thermal heating at depth. The contradiction with our results is only apparent. At fast subduction rate (8 cm/yr in this case), bending faults do not reside for a long time in the "hydration" window (0.3 to 0.7 Myr Ranero et al., 2003), and heat will distribute within the cold wedge once the lithosphere has reached the trench. More data is needed at slow subductions to test this hypothesis.

5. Conclusion

Among the physical mechanisms that may be responsible for the high heat flow in the actively deforming Central Indian Basin, our models indicate that exothermic serpentinization is the only process that leads to a significant amount of heat release. In contrast to friction-related release of heat, the exothermic serpentinization model is by essence transient and delivers a pulse of extra heat that will rapidly decay with time once serpentinization is completed. We quantitatively show that a pulse of serpentinization in the Central Indian Basin that would have started with the onset of the intraplate deformation there is compatible with the present-day surface heat flow which is 25–30 mW/m^2 above normal, provided a million year delay for the establishment of a mature hydrothermal circulation and a high enough thermal efficiency of the hydration reactions. The moderate transient temperature anomaly is followed by a definitive weakening of the CIB fault network due to the low friction coefficient of partially serpentinized peridotites (Escartin et al., 1997, 2001). In the Wharton Basin, the thermal pulse has already passed, in relation to a totally different geometry of the fault network (widely-spaced vertical strike-slip faults rather that closely spaced reverse faults). The enigmatic bright reflectors that we imaged in the CIB on multichannel seismic profiles at depth of 8 to 15 km below the top of the crust coincide with the location of the maximum reaction rate coefficient of serpentinization in our model. They are likely to result from serpentinization fronts propagation at mantle depth. Our results suggest that pulses of serpentinization within the oceanic lithosphere result in transient rheology that breaks the age-dependent mechanical strength law: this mechanism may have been responsible in the past for sudden plate reorganizations at global scale, and it may also explain the abnormally low rigidity found today for some of the oldest oceanic plates (Bry and White, 2007; Korenaga, 2007).

Acknowledgements

We thank three anonymous reviewers for their constructive reviews and the editor Claude Jaupart for his stimulating comments. Phèdre multichannel lines were reprocessed with the GeoCluster seismic software of CGGVeritas in the framework of the Enabling Grids for E-sciencE project, co-funded by the European Commission through the Sixth Framework Programme (http://www.eu-egee.org).

References

Bry, M., White, N., 2007. Reappraising elastic thickness variation at oceanic trenches. J. Geophys. Res. 112, B08414. doi:10.1029/2005JB004190.
Bull, J.M., Scrutton, R.A., 1990a. Sediment velocities and deep structure from wide angle reflection data around Leg 116 sites. Proc. Ocean Drill. Prog. Sci. Results 116, 311–316.
Bull, J.M., Scrutton, R.A., 1990b. Fault reactivation in the central Indian Ocean and the rheology of oceanic lithosphere. Nature 344, 855–858.
Bull, J.M., Scrutton, R.A., 1992. Seismic reflection images of intraplate deformation, Central Indian Basin, and their tectonic significance. J. Geol. Soc. 149, 955–966.
Ćadek, O., Fleitout, L., 2003. Effect of lateral viscosity variations in the top 300 km on the geoid and dynamic topography. Geophys. J. Int. 152, 566–580.
Carslaw, H.S., Jaeger, J.C., 1959. Conduction of Heat in Solids. Oxford University Press, New York. 510 pp.
Chamot-Rooke, N., Jestin, F., De Voogd, B., the Phèdre Working Group, 1993. Intraplate shortening in the central Indian Ocean determined from 2100-km-long north–south deep seismic reflection profile. Geology 21, 1043–1046.
Christensen, N.I., 2004. Serpentinites, peridotites, and seismology. Int. Geol. Rev. 46, 795–816.
Cochran, J.R., et al., 1989. Intraplate deformation and Bengal Fan sedimentation: background and objectives. Proc. Ocean Drill. Program, Initial Rep. 116, 3–11.
Contreras-Reyes, E., Grevemeyer, I., Flueh, E.R., Scherwath, M., 2007. Alteration of the subducting oceanic lithosphere at the southern central Chile trench-outer rise. Geochem. Geophys. Geosys. 8, Q07003. doi:10.1029/2007GC001632.
Crosby, A.G., McKenzie, D., Sclater, J.G., 2006. The relationship between depth, age and gravity in the oceans. Geophys. J. Int. 166, 553–573. doi:10.1111/j.1365-246X.2006.03015.x.
D'Alessio, M.A., Williams, C.F., Burgmann, R., 2006. Frictional strength heterogeneity and surface heat flow: implications for the strength of the creeping San Andreas fault. J. Geophys. Res. 111, B05410. doi:10.1029/2005JB003780.
Delescluse, M., Chamot-Rooke, N., 2007. Instantaneous deformation and kinematics of the India–Australia plate. Geophys. J. Int. 168, 818–842. doi:10.1111/j.1365-246X.2006.03181.x.
Delescluse, M., Montési, L.G.J., Chamot-Rooke, N., 2008. Fault reactivation and selective abandonment in the oceanic lithosphere. Geophys. Res. Lett. 35, L16312. doi:10.1029/2008GL035066.
Deplus, C., Diament, M., Hébert, H., et al., 1998. Direct evidence of active deformation in the eastern Indian oceanic plate. Geology 26 (2), 131–134.
Emmanuel, S., Berkowitz, B., 2006. Suppression and stimulation of seafloor hydrothermal convection by exothermic mineral hydration. Earth Planet. Sci. Lett. 243, 657–668.
Escartin, J., Hirth, G., Evans, B., 1997. Effects of serpentinization on the lithospheric strength and the style of normal faulting at slow spreading ridges. Earth Planet. Sci. Lett. 151, 181–189.
Escartin, J., Hirth, G., Evans, B., 2001. Strength of slightly serpentinized peridotites: implication for the tectonics of oceanic lithosphere. Geology 29 (11), 1023–1026.
Francis, T.J.G., 1981. Serpentinization faults and their role in tectonics of slow spreading ridges. J. Geophys. Res. 86, 11616–11622.
Fruh-Green, G.L., Kelley, D.S., Bernasconi, S.M., Karson, J.A., Ludwig, K.A., Butterfield, D.A., Boschi, C., Proskurowski, G., 2003. 30,000 years of hydrothermal activity at the lost city vent field. Science 301, 495–498.
Fyfe, W.S., 1974. Heats of chemical reactions and submarine heat production. Geophys. J. R. Astron. Soc. 37, 213–215.
Geller, C.A., Weissel, J.K., Anderson, R.N., 1983. Heat transfer and intraplate deformation in the Central Indian Ocean. J. Geophys. Res. 88, 1018–1032.
Gerbault, M., 2000. At what stress level is the central Indian Ocean lithosphere buckling? Earth Planet. Sci. Lett. 178, 165–181.
Gordon, R.G., DeMets, C., Argus, D.F., 1990. Kinematic constraints on distributed lithospheric deformation in the equatorial Indian-ocean from present motion between the Australian and Indian plates. Tectonics 9 (3), 409–422.
Grevemeyer, I., Kaul, N., Diaz-Naveas, J.L., Villinger, H.W., Ranero, C.R., Reichert, C., 2005. Heat flow and bending-related faulting at subduction trenches: case studies of Nicaragua and Central Chile. Earth Planet. Sci. Lett. 236, 238–248.
Grevemeyer, I., Ranero, C.R., Flueh, E.R., Klaschen, D., Bialas, J., 2007. Passive and active seismological study of bending-related faulting and mantle serpentinization at the Middle America trench. Earth Planet. Sci. Lett. 258, 528–542. doi:10.1016/j.epsl.2007.04.013.
Jestin, F., (1994). Cinématique rigide et déformations dans la jonction triple Afar et dans le Bassin Indien Central. PhD thesis, Université Paris VI.
Kelley, D.S., Karson, J.A., Blackman, D.K., Fruh-Green, G.L., 2001. An off-axis hydrothermal vent field near the Mid Atlantic Ridge at 30 degrees N. Nature 412, 145–149.
Korenaga, J., 2007. Thermal cracking and the deep hydration of oceanic lithosphere: a key to the generation of plate tectonics? J. Geophys. Res. 112, B05408. doi:10.1029/2006JB004502.
Krishna, K.S., Bull, J.M., Scrutton, R.A., 2001. Evidence for multiphase folding of the Central Indian Ocean lithosphere. Geology 29 (8), 715–718.
Krishna, K.S., Gopala Rao, D., Neprochnov, Y.P., 2002. Formation of diapiric structure in the deformation zone, Central Indian Ocean: a model from gravity and seismic reflection data. Proc. Indian Acad. Sci. 111, 17–28.
Lachenbruch, A.H., Sass, J.H., 1980. Heat flow and energetics of the San Andreas fault zone. J. Geophys. Res. 85, 6185–6222.
Lachenbruch, A.H., Sass, J.H., 1992. Heat flow from Cajon Pass, fault strength, and tectonic implications. J. Geophys. Res. 97, 4995–5015.
Levchenko, O.V., Verzhbitsky, E.V., 2003. Structural aspects of the intraplate deformations of the oceanic crust north of the Afanasy Nikitin rise (Indian Ocean. Oceanology 43 (6), 840–851.
Louden, K.E., 1995. Variation in crustal structure related to intraplate deformation: evidence from seismic refraction and gravity profiles in the Central Indian Basin. Geophys. J. Int. 120, 375–392.

Lowell, R.P., Rona, P.A., 2002. Seafloor hydrothermal systems driven by the serpentinization of peridotite. Geophys. Res. Lett. 29 (26), 1–4.
MacDonald, A.H., Fyfe, W.S., 1985. Rate of serpentinization in seafloor environments. Tectonophysics 116, 123–135.
O'Hanley, D.S., 1992. Solution to the volume problem in serpentinization. Geology 20, 705–708.
Okal, E.A., 1983. Oceanic intraplate seismicity. Annu. Rev. Earth Planet. Sci. 11, 195–214.
Ormond, A., Boulègue, J., Genthon, P., 1995. A thermoconvective interpretation of heat flow data in the area of Ocean Drilling Program Leg 116 in a distal part of the Bengal Fan. J. Geophys. Res. 100, 8083–8095.
Pollack, H.N., Hurter, S.J., Johnson, J.R., 1993. Heat flow from the earth's interior: analysis of the global data set. Rev. Geophys. 31 (3), 267–280.
Ranero, C.R., Phipps Morgan, J., McIntosh, K., Relchert, C., 2003. Bending-related faulting and mantle serpentinization at the Middle America trench. Nature 425, 367–373.
Sandwell, D.T., Smith, W.H.F., 1997. Marine Gravity from Geosat and ERS-1 Altimetry. J. Geophys. Res. 102, 10039–10054.
Scholz, C.H., 2000. Evidence for a strong San Andreas fault. Geology 28 (2), 163–166.
Shipboard Scientific Party, 1989. Site 718: Bengal Fan. In: Cochran, J.R., Stow, D.A.V., et al. (Eds.), 1988 Proc. ODP, Init. Repts., College Station, TX (Ocean Drilling Program), vol. 116, pp. 91–154.
Stein, C.A., Weissel, J.K., 1990. Constraints on the Central Indian Basin thermal structure from heat flow, seismicity and bathymetry. Tectonophysics 176, 315–332.
Stein, C.A., Hobart, M.A., Abbott, D.A., 1988. Has the Wharton Basin's heat flow been perturbed by the formation of a diffuse plate boundary in the Indian Ocean? Geophys. Res. Lett. 15, 455–458.
VanOrman, J., Cochran, J.R., Weissel, J.K., et al., 1995. Distribution of shortening between the Indian and Australian plates in the Central Indian Ocean. Earth Planet. Sci. Lett. 133, 35–46.
Verzhbitsky, E.V., Lobkovsky, L.I., 1993. On the mechanism of heating-up of the Indo-Australian plate. J. Geodyn. 17, 27–38.
Verzhbitsky, E.V., Neprochnov, Y.P., 2005. Deep structure of the central Indian Ocean inferred from geophysical data. Geotectonics 39 (3), 213–223.
Wang, K., Mulder, T., Rogers, G.C., Hyndman, R.D., 1995. Case for very low coupling stress on the Cascadia subduction fault. J. Geophys. Res. 100, 12907–12918.
Weissel, J.K., Anderson, R.N., Geller, C.A., 1980. Deformation of the Indo-Australian plate. Nature 287, 284–291.
Williams, C.F., 1990. Hydrothermal circulation and intraplate deformation: constraints and predictions from in-situ measurements and mathematical models. In: Cochran, J.R., Stow, D.A.V., et al. (Eds.), Proc. ODP, Sci. Results, 116:College Station, TX (Ocean Drilling Program), pp. 345–359.
Wiens, D.A., Stein, S., DeMets, C., Gordon, R.G., Stein, C., 1986. Plate tectonic models for Indian-Ocean intraplate deformation. Tectonophysics 132, 37–48.
Ziolkowsky, A., Hanssen, P., Gatliff, R., Jakubowicz, H., Dobson, A., Hampson, G., Li, X.Y., Liu, E., 2003. Use of low frequencies for sub-basalt imaging. Geophys. Prospect. 51 (3), 169–182.